Available online at www.sciencedirect.com
SCIENCE DIRECT®
Journal of Sound and Vibration 282 (2005) 713–733
JOURNAL OF SOUND AND VIBRATION
www.elsevier.com/locate/jsvi

Experimental study on active vibration control of a gearbox system

Yuan H. Guan[a], Teik C. Lim[b,*], W. Steve Shepard, Jr.[a]

[a]*Department of Mechanical Engineering, University of Alabama, 290 Hardaway Hall, Box 870276 Tuscaloosa, AL 35487, USA*
[b]*Department of Mechanical, Industrial and Nuclear Engineering, University of Cincinnati, 624 Rhodes Hall, P.O. Box 210072, Cincinnati, OH 45221, USA*

Received 26 August 2003; accepted 7 March 2004
Available online 12 October 2004

Abstract

An active internal gearbox structure is developed and evaluated experimentally to suppress gear pair vibration due to transmission error excitation. The approach is based on an active shaft transverse vibration control concept that was theoretically analyzed in an earlier study and determined to be one of the most feasible methods. The system comprises of a piezoelectric stack actuator for applying control forces to the shaft via a rolling element-bearing, and a highly efficient, enhanced delayed-x LMS control algorithm to generate the appropriate control signals. To avoid the aliasing effects of higher frequency signals and reduce the phase delay of conventional filters, a multi-rate minimum-phase low-pass digital filter is also integrated into the controller. The experimental results yield 8–13 dB attenuation in the gearbox housing vibration levels and correspondingly 5–8 dB reduction in measured gear whine noise levels at the first and second operating gear mesh frequencies.

1. Introduction

The gear pair assembly remains one of the major noise and vibration sources in power transmission systems typically used in automotive, aerospace and industrial applications. The

*Corresponding author. Tel.: +1-513-556-4450; fax: +1-513-556-3390.
E-mail address: teik.lim@uc.edu (T.C. Lim).

0022-460X/$ - see front matter © 2004 Elsevier Ltd. All rights reserved.
doi:10.1016/j.jsv.2004.03.043

gear vibration and noise signatures are often dominated by several high-level tonal peaks that occur at the fundamental gear mesh frequency (given by the product of the shaft speed and number of gear teeth) and its harmonics. The primary forcing function is produced by the gear transmission error excitation resulting from tooth profile errors, misalignment and elastic deformation [1,2]. The excessive dynamic response generated can frequently lead to structural fatigue failure and severe annoyance. Therefore, it is highly desirable to reduce the gear vibration and noise levels. To achieve this goal, the present study demonstrates the use of an active internal gearbox structure to treat the gear excitation source more directly. Details of the actuation concept employed in this study will be presented later. In this implementation, the dynamic characteristics of the gearbox and active vibration control system are assumed to be linear, which is especially valid when the transmitted load and damping levels are sufficiently high, and the operating mesh frequency is well below the gear pair torsion resonance. The highly deterministic nature of the discrete narrowband gear tones makes the gearbox system a suitable candidate for active vibration control study in spite of the complexity in the vibration generation and transmissibility processes. A review of recent active vibration and acoustic noise control investigations that are relevant to gear dynamics is discussed next.

One of the earliest investigations applying active control to tackle the gear mesh vibration problem was done in 1994 by Montague et al. [3], who applied configurations that consisted of one and two piezoelectric actuators mounted onto one and both shafts separately. Their setup employed an analog phase shifter with an amplifier to drive the actuators. Up to 70% reduction in gear mesh vibrations was reported in their experiments. However, only the fundamental gear mesh frequency was controlled, and the phase shifter and amplifier had to be manually adjusted to obtain the desired drive signal. This control process is tedious since the manual tuning procedure must be performed at each rotation speed and running condition. In 1999, Rebbechi, et al. [4] tried a similar approach using a pair of magnetostrictive actuators with an adaptive digital controller to treat the responses at the first three mesh harmonics simultaneously. A reduction of 20–28 dB was reported at the fundamental mesh frequency, while reductions of only 2–10 dB were achieved at the higher harmonics. In that piece of work, they used a conventional filtered-x least mean square (LMS) algorithm that required a relatively accurate estimation of the secondary path transfer function over a wide frequency range. Note that this secondary path represents the dynamic characteristic between the control input and error signal. The level of accuracy needed will generally require a large-order finite impulse response (FIR) model of the secondary path and thus lead to fairly high computational load requirement. Later, Chen and Brennan [5] developed an active vibration control scheme that uses three magnetostrictive actuators mounted directly on one of the gears in order to produce circumferential forces for suppressing steady-state torsional vibrations. The experimental results showed about 7 dB of reduction in gear angular vibrations at the fundamental tooth meshing frequency of 250 Hz.They applied a frequency domain adaptive harmonic controller that is actually designed for nonlinear systems even though it is also applicable for cases with multiple harmonic responses [6]. More recently, Guan et al. [7] proposed a new direct hybrid adaptive controller to tackle gear pair torsional and translational vibrations simultaneously by using several inertial actuators on both gear bodies. However, this actuation concept requires the use of complex slip ring configuration to transfer power signals to the rotating actuators and also other major structural modifications.

To identify an optimum actuator setup, four potentially feasible actuation concepts aimed to reduce gearbox housing vibrations due to transmission error excitation were modeled theoretically and compared by computing the required control forces and amplifier power spectra in another recent study [8]. From that analysis, the active shaft transverse vibration control scheme was identified to be the most suitable approach. Consequently, that same approach will also be used for the application in this work. Other than these studies, no other work on the active vibration control of internal gearbox components is found in the public domain literature. However, there have been several active vibration control studies that treated the structural supports outside the gearbox [9–12] in order to reduce vibration transmissibility. In particular, Balachandran and his co-workers [10,11] analytically and numerically studied the control of both longitudinal and flexural vibration transmissibilities through a helicopter gearbox strut by using piezoelectric stack and magnetostrictive actuators separately. They concluded that piezoelectric stack actuators are well suited for controlling flexural wave transmission through the gearbox strut. However, one of the limitations of these external actuation techniques is that they can only treat specific structure-borne paths and have virtually no impact on the air-borne path. Furthermore, the points of control force applications are located quite far away from the gear pair, which essentially provides no effect on the excitation source.

To apply active vibration control in a gearbox, two primary issues on actuation concept and control algorithm must be addressed. The selection of a suitable actuation concept has been discussed previously [8]. As noted above, the proposed system comprises of an active shaft transverse vibration control scheme that will be studied experimentally in this paper. This technique uses a piezoelectric linear stack actuator to deliver control forces to the rotating shaft close to the gear pair via a rolling element bearing. Further description of the structural design will be given in the next section. On the second issue related to the control algorithm, concerns are mainly on the efficiency and performance of the controller. Although the conventional filtered-x LMS algorithm is one of the most widely used techniques, it requires the availability of a relatively accurate secondary path transfer function over a wide frequency range, as discussed above. Moreover, the computational load can be quite high especially for large and complicated applications. Since the target signals in the gearbox vibration problem are the discrete gear mesh harmonics, it is more appropriate to apply a simplified delayed-x LMS version. Because the simplified approach aims only at the specific harmonic responses of interest, less computational effort is needed. Furthermore, the geared rotor system can be usually considered to be linear especially under sufficiently high torque, high damping and small backlash conditions. The same linear behavior is expected in the active gearbox structure considered here especially if the piezoelectric stack actuator operates only within a small driving voltage range. Accordingly, the use of a more complex nonlinear controller such as the frequency domain adaptive harmonic controller is not necessary in the present application. Due to the expected hardware implementation difficulties, the hybrid direct adaptive controller [7] is also not selected for this work. Finally, in the attempt to avoid the aliasing effects due to the presence of higher frequency signals as well as to reduce the phase delay in conventional filters, a multi-rate minimum-phase digital FIR filter is integrated into the proposed controller. Using the specific actuation and control elements described here, an experimental active vibration control system for use inside a gearbox is developed. The experiments conducted provide a verification of the effectiveness of the proposed active vibration control concept to control both the fundamental mesh response and its second harmonic under steady-state operating conditions.

2. Active gearbox structure design

The aim of this active vibration control work is to tackle in a more direct manner the gearbox noise and vibration responses due to transmission error excitation originating from the mesh point. The transmission error interacts with the gear train system dynamic characteristics to generate the tooth mesh force that in turn excites the torsional and lateral shaft motions. The resulting vibration energy is then transmitted through the bearings, and into the housing and support structures, where some of this energy is ultimately radiated as high-frequency gear whine noise that most people find annoying. Additionally, the resultant structural vibration can accelerate fatigue damage. Hence, to deal with both the mesh force generation and vibration transmissibility processes more effectively, the control force must be applied close to the gear pair. This close proximity will allow the application of a single controller, with the potential to simultaneously suppress both gear housing vibration and radiated acoustic noise [8]. The results strongly favor an approach that is based on the active shaft transverse vibration control scheme as it theoretically requires the least actuation effort and avoids the use of a complex slip ring setup as noted earlier. This actuation concept is further developed in this study as described next.

To demonstrate the feasibility of the active shaft transverse vibration control concept, a direct-drive power-absorbing-type test gearbox was constructed [13]. The cross section of the setup is schematically shown in Fig. 1 and the physical test rig is illustrated in Fig. 2. The basic setup consists of a 2-hp AC electric drive motor, a torque transducer, a gearbox with a 1:1 ratio spur gear pair, and a 2-hp DC dynamometer connected to a bank of power resistors that act as a load. Each gear has 60 teeth and a 3-in pitch diameter. Thus, if the gear pair rotates at 300 rpm (revolution per minute), the fundamental gear mesh frequency is 300 Hz, the next harmonic is

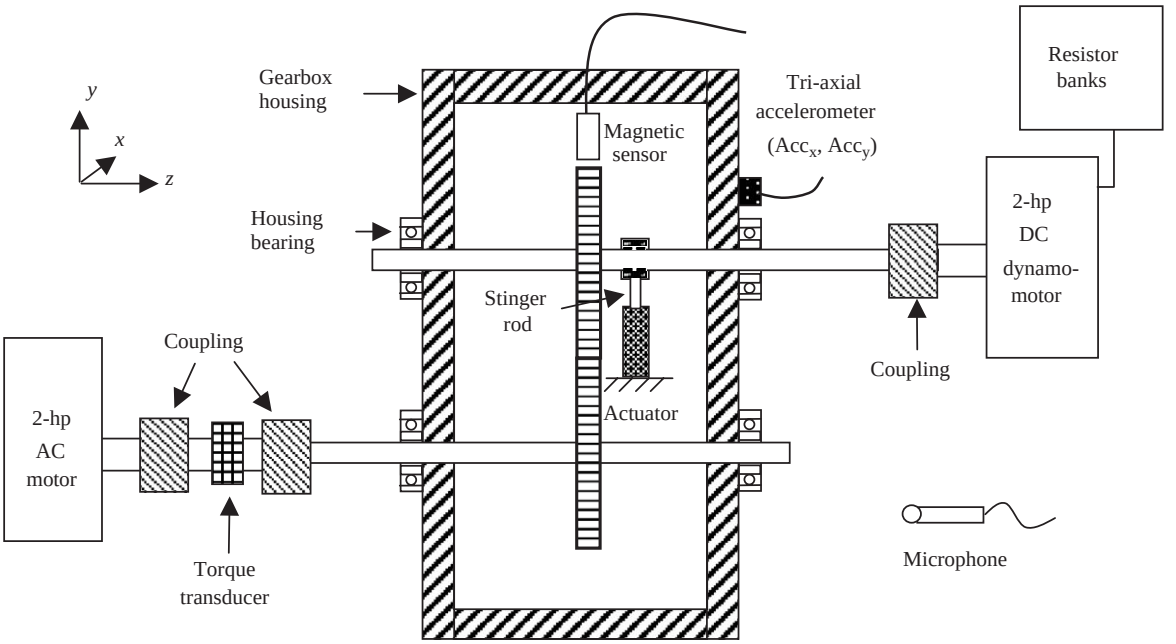

Fig. 1. A cross-section of the active gearbox vibration control setup.

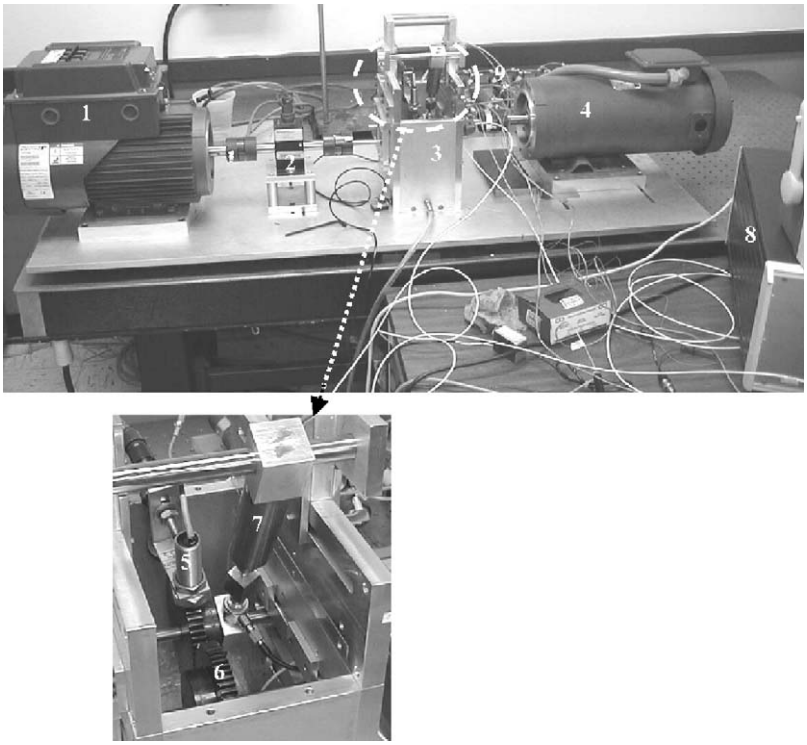

Fig. 2. Experimental setup of the active gearbox vibration control system: (1) AC drive motor; (2) torque transducer; (3) gear housing; (4) DC load dynamometer; (5) magnetic rotation pulse sensor; (6) gear pair; (7) piezoelectric stack actuator; (8) piezoelectric amplifier; (9) resistor banks.

600 Hz and so on. A magnetic sensor is installed in the proximity of the driven gear tooth to pick up the rotation pulse train, which generates 60 pulses per shaft revolution. A tri-axial accelerometer is attached to the gearbox housing just above the driven shaft bearing facing the DC load dynamometer. The x and y axes of the accelerometer are perpendicular and parallel to the gear mesh line-of-action, respectively. The y-axis signal from the accelerometer (labeled as Acc_y) is used as the error signal for the controller, while the x-axis signal (labeled as Acc_x) is used to measure the housing vibration perpendicular to the gear mesh line-of-action. A microphone is also placed besides the gearbox as depicted in Fig. 1 to monitor the radiated gear whine noise level.

A piezoelectric stack actuator, driven by a high-voltage amplifier that receives command signals computed by the controller, is connected to the driven shaft via a needle bearing, as shown fully in Fig. 1 and partially in Fig. 2. Note that it is beyond the scope of this paper to analyze the optimum placement of the actuator relative to the gear pair. For the present analysis, the actuator is positioned on the shaft at one-third of the length from the gear to the housing support location. The selection of this location is based primarily on packaging considerations. The actuation direction is positioned parallel to the gear mesh line-of-action, such that the active control force is better able to disrupt the mesh force generation and vibration transmissibility. Also, note that a proper preload level must be set when mounting the actuator. This is because, if the preload is too

small, the actuator may not be able to produce both compressive and tensile bending force on the shaft due to clearances in the setup. On the other hand, if the preload is too large, the shaft will bend excessively. This will lead to an undesirably high level of eccentricity in the gears, which further complicates the vibration control problem. As a result, the preload level can be determined by estimating the required tensile bending force on the shaft, as discussed previously [8], and by minimizing the clearances in the assembly to avoid further eccentricity in the gears. To compensate for possible run-out and excessive shaft deflection that can generate harmful lateral forces in the actuator, a thin stinger rod that is stiff in the longitudinal direction and relatively flexible in the transverse direction is attached to one end of the actuator. The underlying control algorithm that forms the core of the control system is presented in the next section.

3. Adaptive controller

In the proposed experimental implementation, the adaptive delayed-x LMS control law [14] is applied as noted above. One of the main advantages of this control scheme is the low computational effort required as the reference signal is not filtered by the generally large-order impulse response model of the secondary path. In fact, this delayed-x LMS control theory is a simplified form of the filtered-x LMS algorithm in that it models the secondary path as a gain attenuator and a phase delay element at each harmonic frequency, and ignores the transfer function at other frequencies. Even though this proposed controller has been applied to numerous broadband and narrowband active noise control applications [15,16], it has not been used or tested for gear vibration control. A schematic of the delayed-x LMS control theory used in this experiment is shown in Fig. 3. Here, the secondary path transfer function from the input voltage of the actuator amplifier to the gear housing vibration is given by H_2, which is represented at one operating gear mesh frequency as $gZ^{-\Delta}$, where g is the gain attenuation and Δ is the number of the unit delay symbolized by Z^{-1}. The unwanted disturbance d is the uncontrolled gearbox housing vibration due to the tooth mesh forcing function resulting from the transmission error excitation. The output function y is the portion of housing response caused by the applied force from the actuator. Hence, the error signal e is the total housing response, which can be measured directly. The reference signal r is provided by either the gear rotation pulse train or a manually generated sinusoidal signal, and the control weights W represent a finite impulse response (FIR) filter with n

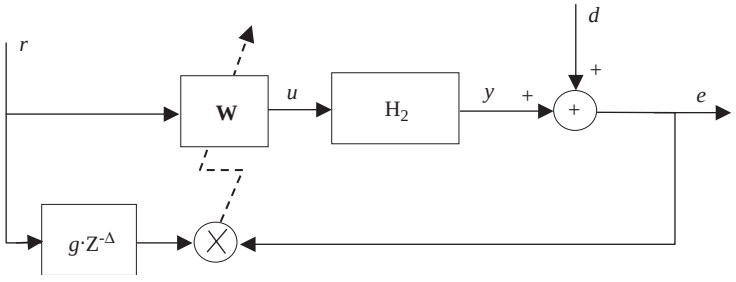

Fig. 3. Block diagram of the conventional delayed-x LMS algorithm.

taps. The control law of the delayed-x LMS algorithm [14] can be given by the relationship

$$W(k+1) = W(k) + 2\mu e(k)R(k-\Delta), \tag{1}$$

where k is the time index, R is the tap-delayed of the reference signal r, and μ is the step size that already includes the gain attenuation g of the secondary path transfer function. In practice, it is often useful to use a leaky LMS algorithm [17] to update the controller weight in order to increase the stability of the closed-loop system. Therefore, Eq. (1) can be replaced by

$$W(k+1) = \lambda W(k) + 2\mu e(k)R(k-\Delta), \tag{2}$$

where λ is the leaky coefficient that can range between zero and unity, but often is very close to the value of one.

Although it has been shown in an earlier work [15] that the conventional delayed-x LMS algorithm performs well in a relatively broadband active noise control of long duct systems, its performance is not so good in low signal-to-noise ratio and narrowband cases. In the problem of low signal-to-noise ratio, the convergence rate is quite poor and the control algorithm tends to excite the out-of-band overshoot. This deterioration in the control performance is due to the fact that the simplification of the secondary path transfer function into a phase delay and gain attenuation at each harmonic will produce a modeling error at other frequencies [18]. To overcome these deficiencies, an improved delayed-x LMS algorithm shown in Fig. 4 is applied in this implementation. The two improvements added to this algorithm are discussed next.

The first improvement in the basic control algorithm involves adding an adaptive line enhancer [19] between the reference signal r and the measured error signal e as illustrated in Fig. 4. The weight W_2 of the adaptive line enhancer is actually a second-order FIR structure. At steady state and when the step size of the enhancer is small, the enhancer can be shown to be equivalent to a very narrow, band-pass second-order infinite impulse response (IIR) filter. The enhancer also yields two salient features of unity gain and zero-phase delay at the frequency point very close to the reference frequency [20] under steady-state conditions. Consequently, the adaptive line enhancer can be applied to filter out all frequency components, except for the reference frequency without introducing any additional phase delay. Although a traditional

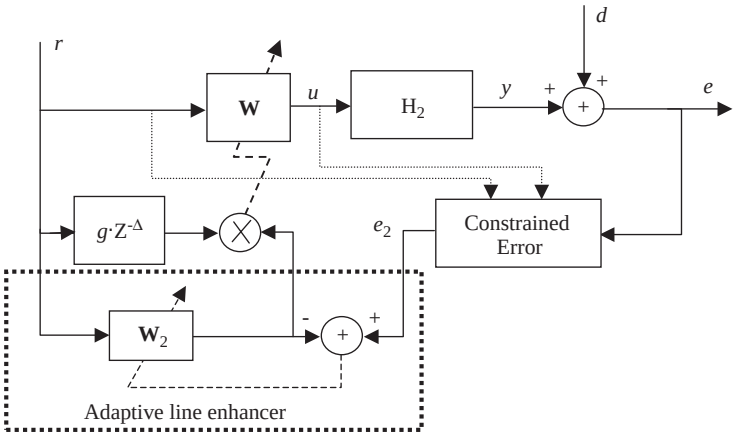

Fig. 4. Block diagram of the improved delayed-x LMS algorithm.

band-pass filter could be applied to reduce unwanted frequency components, the traditional filter increases the phase delay of the secondary path and deteriorates the active vibration control system performance. Furthermore, with a cleaner error signal at each harmonic frequency, which is provided by the adaptive line enhancer, the spillover (out-of-band overshoot) problem within the disturbance pass band frequency range can be avoided [20]. As a result, the adaptive line enhancement described here can directly provide the adaptive law of Eqs. (1) or (2) with a significantly better signal-to-noise ratio, cleaner error signal, and reduction of the out-of-band overshoot. It is worthwhile to note that the controller described in Ref. [21] can also be applied to address the spillover problem. However, since it is not an adaptive controller, it is not useful to the current application and hence not discussed more in detail here.

The second improvement implemented in this study involves constraining the fundamental structure of the error signal. This constrained structure compensates for the possible delay in the secondary path which otherwise limits the largest stable step size of the controller. If the secondary path is modeled as $gZ^{-\Delta}$, then assuming randomness and stationary behavior of the reference input signal, the stable range of the step size is given by [22]

$$0<\mu<\frac{1}{g^2\lambda_{\max}}\sin(\pi/(4\Delta+2)), \tag{3}$$

where $\lambda_{\max}$ represents the maximum eigenvalue of the autocorrelation matrix of the reference signal. However, by applying the constrained structure, a new error signal e_2 that is similar to the results in Ref. [23] can be shown to be

$$e_2(k)=e(k)-gu(k-\Delta)+R(k)^{\mathrm{T}}W(k), \tag{4}$$

where $u(k)=R(k)^{\mathrm{T}}W(k)$ is the present control signal. This then produces a new stable step size range given by

$$0<\mu<\frac{1}{g^2\lambda_{\max}}. \tag{5}$$

Note that the stable range of the step size does not depend on the unit delay number Δ. Therefore, the maximum stable step size can be increased dramatically in the case of a large unit delay number Δ when compared to the previous baseline formulation. Equivalently, the larger stable step size used in the controller weights update will increase the convergence rate and improve the vibration reduction performance. The above analysis assumes the reference signal to be random and stationary, while the reference signal in this gearbox application is quasi-periodic. In spite of this slight discrepancy, the analysis can still be applied to guide in the selection of a proper stable step size.

It may be pointed out that the proposed controller is in fact a special form of the well-studied filtered-x LMS algorithm, only with improvements, and is therefore guaranteed to be stable when used with a suitable secondary path transfer function and controller step size. Next, the active vibration control algorithm and the relevant filters are developed to complete the active gearbox vibration control prototype.

4. Filter and code designs

During the development of the setup, it was discovered that the error signal of the current gearbox application, i.e. the measured housing surface vibration, contains very rich high frequency components of up to 8 kHz. An example of the gearbox housing vibration spectrum is shown in Fig. 5 for a shaft speed of 290 rpm.In this figure, the first three operating gear mesh frequencies (labeled as $1\times$, $2\times$ and $3\times$ mesh) are clearly visible. However, the response spectrum also contains a major peak near 8 kHz and fairly significant broadband response around 3–4 kHz. The 8 kHz peak is caused by the gear pair out-of-phase rotation mode, while the broadband spectrum around 3–4 kHz is probably due to the coalescence of numerous housing structural resonances. The interest here is only in controlling the first few operating gear mesh frequencies, such as the first and second harmonics around 290 and 580 Hz, respectively. Consequently, a high stop band reduction low-pass filter is used to remove all the undesirable high-frequency contents.

To meet the above filtering requirements, a digital low-pass filter that is integrated into a PowerPC board is used to simplify the control structure, even though a conventional analog low-pass filter will work. The PowerPC processing board also possesses an analog-to-digital converter to sample the measured dynamic signals and a digital-to-analog converter to generate the analog control signal used to drive the actuator. In order to avoid any aliasing effects in the analog-to-digital converter, a very high sampling frequency, say 20 kHz, is used since vibration components over 10 kHz are rather small and can be neglected. A high-quality FIR digital filter with 80 dB stop band reduction and a corner frequency of 800 Hz is incorporated into the control system

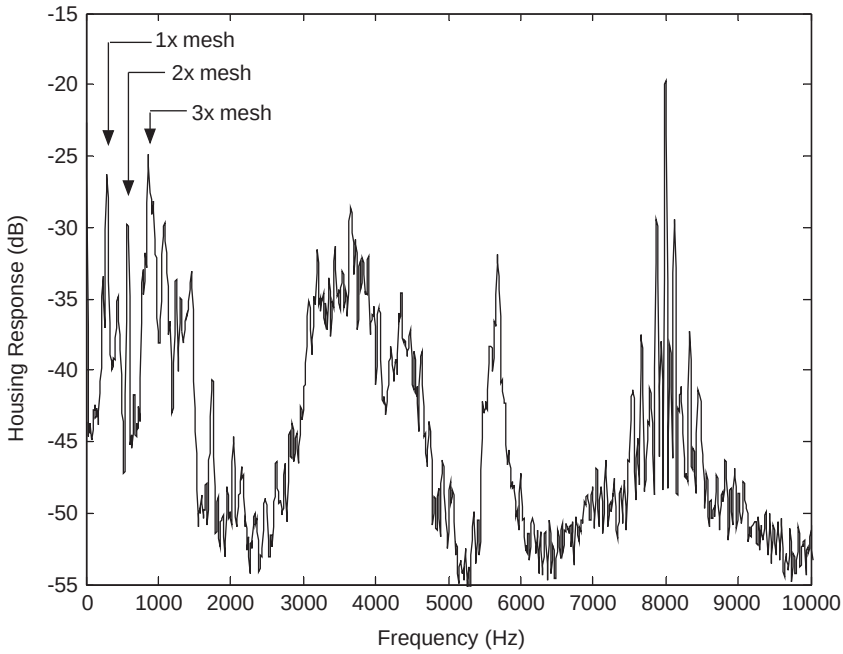

Fig. 5. A typical spectrum of the gearbox housing vibration along the gear mesh line-of-action at 300 rpm (dB re. 1 g).

design. In the final design, the original signal is decimated $\frac{1}{8}$ times to 2.56 kHz, and the controller operating frequency is set at 2.56 kHz as well, which is about 4 times the highest frequency of interest at 650 Hz.Furthermore, to decrease the computational effort of the digital filter, a two-stage multi-rate filter along with an efficient polyphase FIR decimation structure [24] is implemented. The first stage of the proposed filter is an image suppressor with 16 orders and 4 decimation rates. The second stage is actually a model filter with 25 orders and 2 decimation rates. In order to decrease the large group delay of the FIR filter, the two filters are designed to be of minimum-phase types that possess far less delay than traditional linear-phase filters. Fig. 6 compares the performances of the two-stage digital filter and the conventional 8-order analog Butterworth filter having the same corner frequency. Both the magnitude and phase responses are plotted here. The phase delay of the digital filter is almost the same as the analog one in the pass band of interest (0–800 Hz), while the magnitude response in the transition band region (800–1200 Hz) of the digital filter is much sharper than the analog one. In fact, using a linear-phase FIR filter to achieve the same amplitude response will yield a group delay that is at least three times larger than the proposed minimum-phase design. This clearly demonstrates that the new FIR filter outperforms both the analog anti-aliasing and the linear-phase FIR filters for a given set of fixed transition bandwidths.

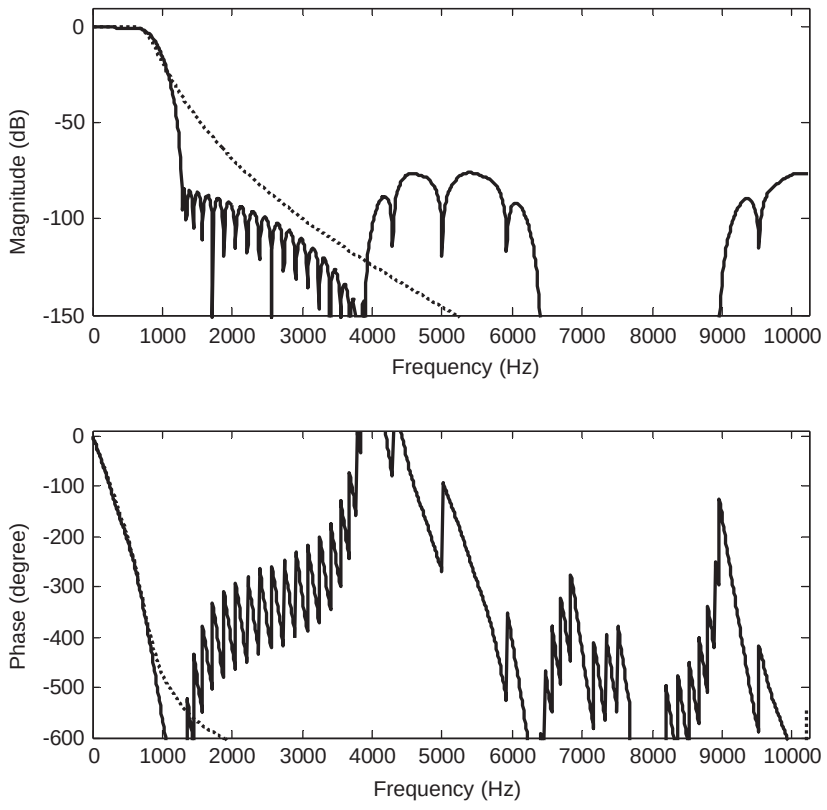

Fig. 6. Comparison of the performances of the digital multi-rate minimum-phase FIR filter (—) and the conventional 8-order Butterworth analog filter (· · · · · ·).

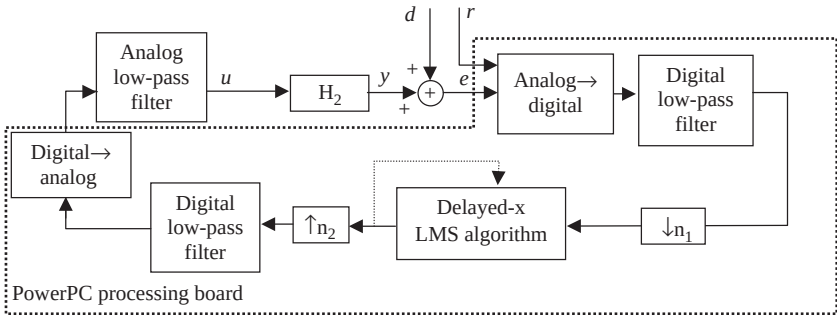

Fig. 7. Block diagram illustrating the implementation of the proposed control theory in a PowerPC processing board.

To reduce the unwanted high-frequency contents of the digital-to-analog converter output, a 4-order low-pass Butterworth analog filter is designed and used as a reconstruction filter. As the transition bandwidth of this 4-order analog filter is not small, a multi-rate low pass digital filter can also be inserted between the calculated control input $u(k)$ and the digital-to-analog converter to improve the filter transition bandwidth. While this multi-rate digital filter is similar to the filter described earlier, it is not necessarily identical. Although this digital filter can remove all the unwanted high frequency components, the analog filter is still needed to remove the zero-order hold effect in the digital-to-analog converter. The complete control diagram, including the relevant filters, is shown in Fig. 7. Here n_1 and n_2 represent two different decimation/interpolation rates. Note that, for clarity, only one stage of the digital FIR filter is shown in the figure. In actuality, a second stage as described above is also present.

The control algorithms and filters are simulated in the Matlab Simulink environment. Its real-time workshop software along with the programmatic interface to the dSPACE DS1104 PowerPC processing board is used to generate the required C codes. Recall that there exist three different operating rates in this application, 20, 5.12 and 2.56 kHz, and thus a multi-tasking schedule has to be used. In order to improve the computational efficiency, the C-coded S-functions are also applied to manually implement some of the critical controller parts, including the control law updates and the proposed adaptive line enhancer implementation. The experimental results of this new closed-loop system will now be presented and discussed.

5. Experimental results

First, the active control of vibrations associated with only the fundamental operating gear mesh frequency is considered. In order to focus on the first gear mesh frequency, a narrower low-pass digital filter with a corner frequency of 400 Hz is used just after the analog-to-digital converter element. Based on this setup, a series of active control experiments are conducted to evaluate the overall performance.

A conventional delayed-x LMS algorithm without any improvement is employed first. This controller possesses a 2-order FIR structure. The reference signal is taken from the gear rotation pulse train that is filtered using the above-mentioned narrow band low-pass digital filter. Fig. 8 illustrates the effect of active vibration control with controller step size $\mu = 0.10$ for the rotation

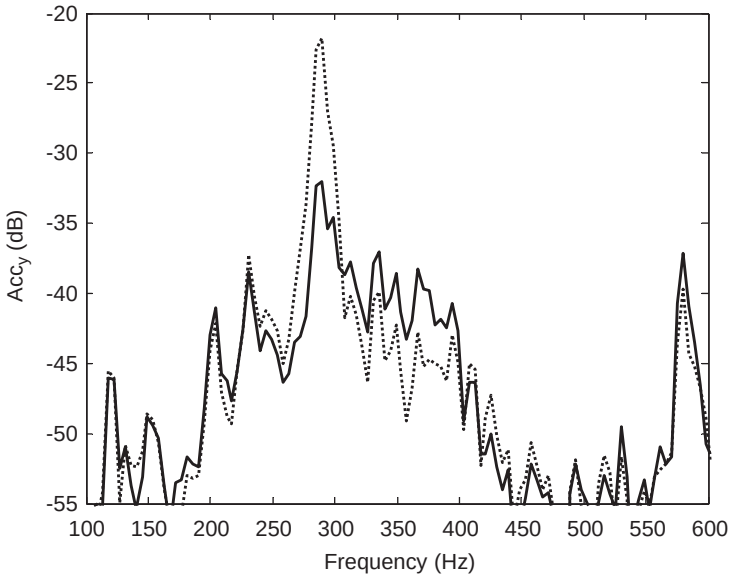

Fig. 8. Effect of the conventional delayed-x LMS algorithm comprising of a 2-order FIR filter on housing vibration response spectrum along the y-axis denoted by Acc_y ($\mu = 0.10$; dB re. 1 g; · · · ·, control off; —, control on).

speed of approximately 290 rpm. About 10 dB of reduction is observed in the response when the active control scheme is applied. Note that the above frequency spectra are calculated from a long time signal, and employ 10 linear averages along with the proper Hanning window. Furthermore, although the active control results shown are from a single run, several different active control experiments performed using the same set of control parameters yield less than 1–2 dB deviation in the measured response relative to the results shown in the figure. This level of repeatability partially supports the validity of the present experimental work. Similar treatments are applied in the following frequency analysis.

The corresponding parts of time history response functions of the housing vibration, the control input voltage applied to the piezo-amplifier, and the weights of the controller for this case are plotted in Fig. 9. Here, it is noticed that as soon as the controller is turned on as time equals 1.4 s, the housing vibrations are immediately reduced. From Fig. 9(b), it is seen that the required control voltage applied to the amplifier is rather small, with a zero-to-peak value of less than 0.3 V. Furthermore, the drive voltage to the piezo-actuator is less than 60 V zero-to-peak (since the amplifier gain is only set to 200), which is well below the potential working level of 500 V. Therefore, the actuator is expected to behave quite linearly, which satisfies the assumption stated earlier. Also, it can be seen in Fig. 9(a) that the uncontrolled housing vibration amplitude is modulated by the shaft rotation speed possibly due to eccentricity in the gear-shaft assembly. In order to compensate for this modulation envelope effect, the controller weights must adapt from time to time, as clearly seen in Fig. 9(c), since a constant weight design will not work well in this case. Also from Fig. 8, some residual gear mesh vibrations around 290 Hz are still present when the controller is operating. These residual vibrations are attributed to the fact that the measured rotational speed is not completely stationary but varies slightly with a standard variance of about

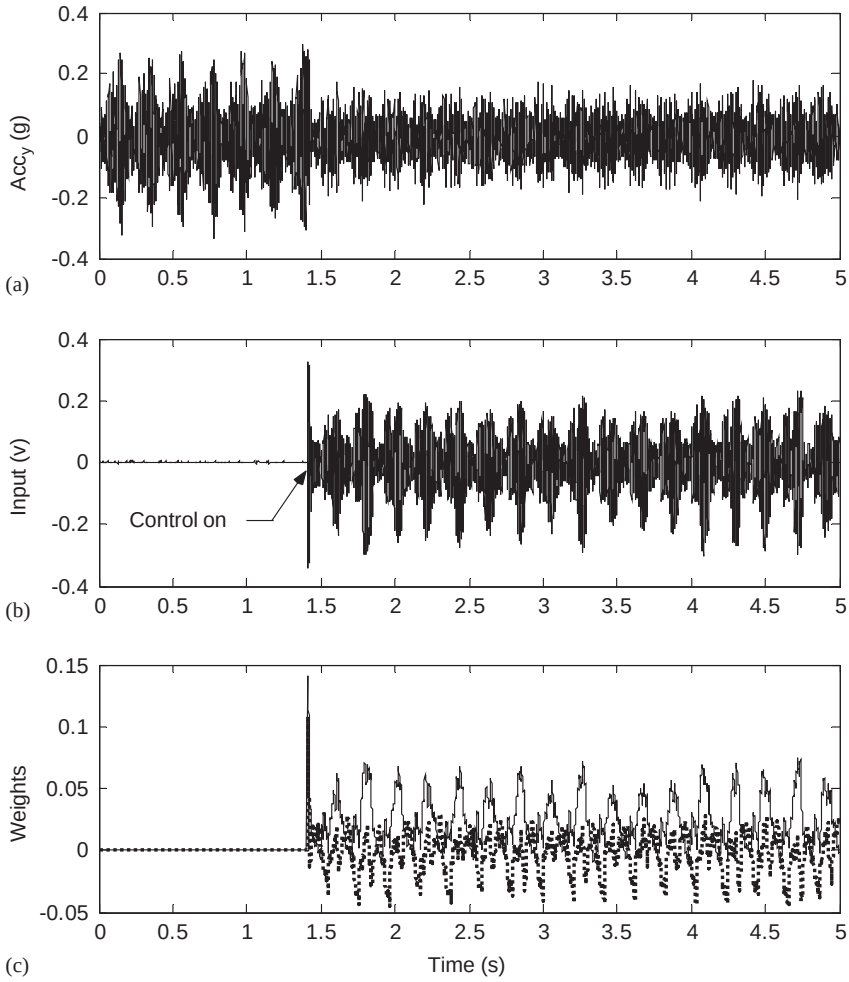

Fig. 9. The corresponding parts of time history response functions of the conventional delayed-x LMS case study given in Fig. 8: (a) housing vibration in the y-axis (error signal); (b) control voltage to the piezoelectric amplifier; (c) first two weights of the controller (—, first weight; ----, second weight).

2.3 rpm, as shown in Fig. 10. Due to the fact that the rotation pulse train is sampled at a fixed rate of 20 kHz, the rotation speed resolution is only 5 rpm, which yields 5 discrete rotation speeds in Fig. 10 (note the two very small bars shown at both ends of the discrete distribution). This implies that both the operating gear mesh frequency and its vibration amplitude are slightly time-varying. Therefore, a fast convergence rate for the controller is needed, which can be accomplished by increasing the control step size μ. Fig. 11 shows the effect of increasing μ from 0.10 to 0.15. In this plot, the attenuation of the housing vibration at 290 Hz is seen to improve from 10 to 12 dB. Unfortunately, the vibration amplitude around 350–400 Hz is amplified when the controller is activated. This typical out-of-band overshoot is caused by too large of a step size μ as discussed in Ref. [25]. In this case, the amplification is primarily due to the effect of the shaft first bending mode near 380 Hz.

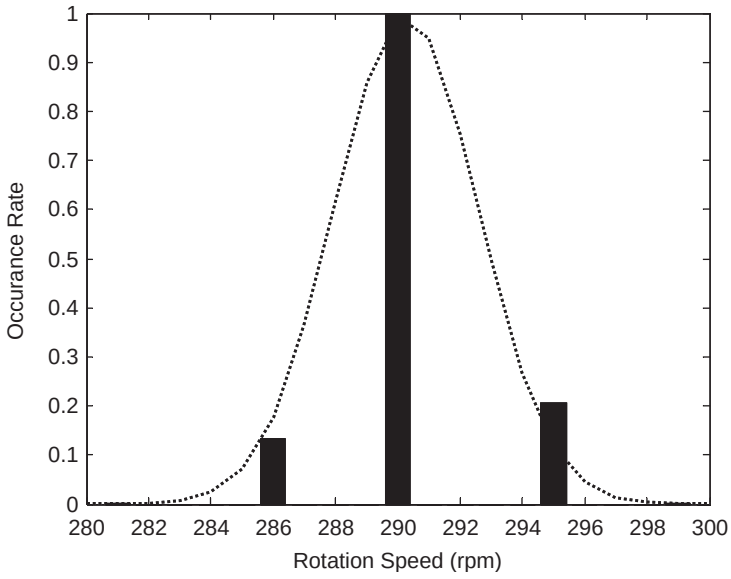

Fig. 10. Measured shaft rotation speed distribution normalized to the mean speed (bar) and Gaussian curve fit (- - -).

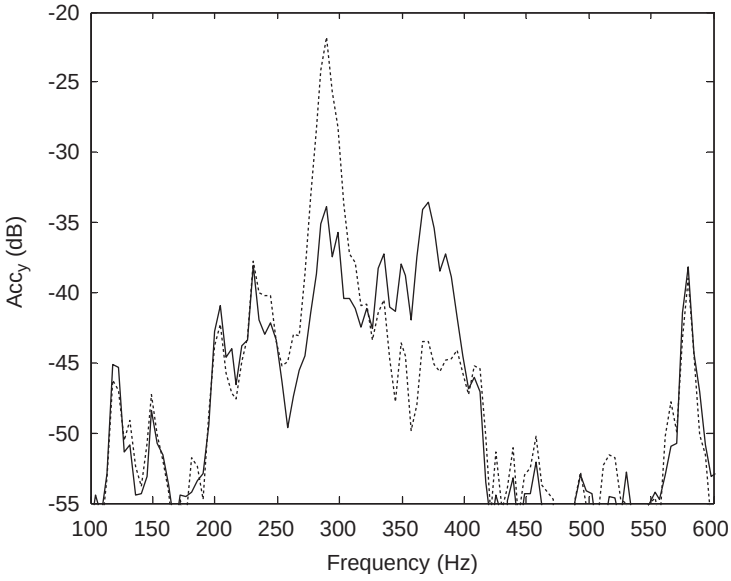

Fig. 11. Effect of the conventional delayed-x LMS algorithm comprising of a 2-order FIR filter on housing vibration response spectrum along the y-axis denoted by Acc_y ($\mu = 0.15$; dB re. 1 g; · · · ·, control off; —, control on).

In order to overcome the out-of-band overshoot problem and increase the convergence rate, the two improvements discussed earlier, namely the adaptive line enhancer and the constrained error structure, are applied. Additionally, the leakage term shown in Eq. (2) is included in the controller

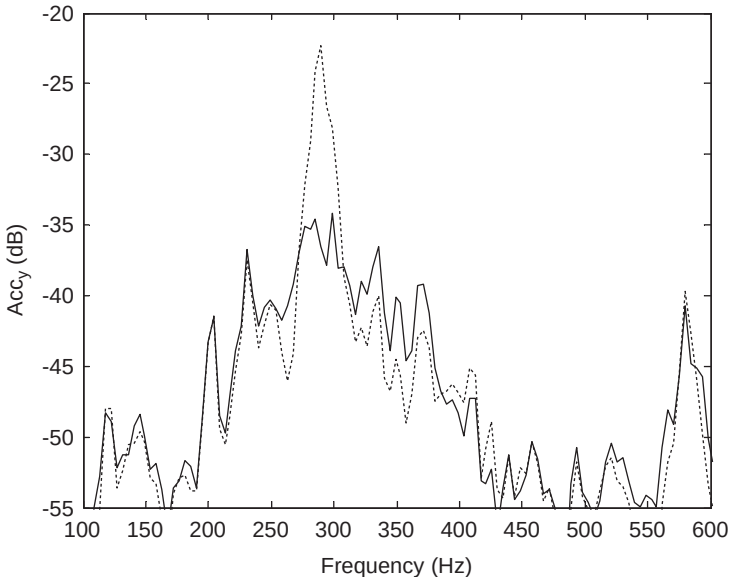

Fig. 12. Effect of the improved delayed-x LMS algorithm comprising of a 32-order FIR filter on housing vibration response spectrum along the y-axis denoted by Acc_y ($\lambda = 0.98$; dB re. 1 g; · · · ·, control off; —, control on).

weights update to improve the stability region. Fig. 12 illustrates the active vibration control result with these added improvements. Here, the leaky coefficient λ is set to 0.98, and the step sizes for the controller and adaptive line enhancer are 0.25 and 0.10, respectively. The order of the controller weight is also increased to 32. Further attenuation of the housing vibration at the 290 Hz mesh frequency is achieved. In fact, as much as 15 dB reduction is attained without obvious out-of-band overshoot or spillover. Within the frequency range of 260–300 Hz, an overall reduction of 13 dB is obtained. The corresponding parts of time history functions of the error signal, control input voltage applied to the actuator amplifier and the first weight of the controller are shown in Fig. 13. From Fig. 13(b), the root-mean-square of the control voltage is nominally 0.12 V. The effect of increasing the leaky coefficient λ from 0.98 to 0.99 is shown in Figs. 14 and 15 for frequency and time domain results. It can be seen in Fig. 14 that the attenuation in housing vibration at the mesh frequency of 290 Hz is further improved to 18 dB. Again, an overshoot problem is present near 370 Hz and the actual reduction in the frequency range of 260–300 Hz is only about 12 dB, which is not as good as the previous case of $\lambda = 0.98$. The root-mean-square value of the control voltage given by Fig. 15(b) increases from 0.12 to 0.18 V. Also, the control voltage is seen to be fairly high during the first few adaptation steps immediately following the activation of the control system at 2.4 s. In fact, the control voltage clips at 0.4 V because a saturation element has been inserted to prevent the amplifier from overdriving the actuator. Actually, the leakage term offers a trade-off between the increase in vibration attenuation and the necessity of a larger control voltage. With a larger leaky coefficient value, better vibration reduction will be achieved and a higher control voltage level will be needed. To clearly view the improvement in the peak reduction performance, a detailed FFT zoom analysis result is shown in Fig. 16. This figure compares the active vibration control performance of the conventional

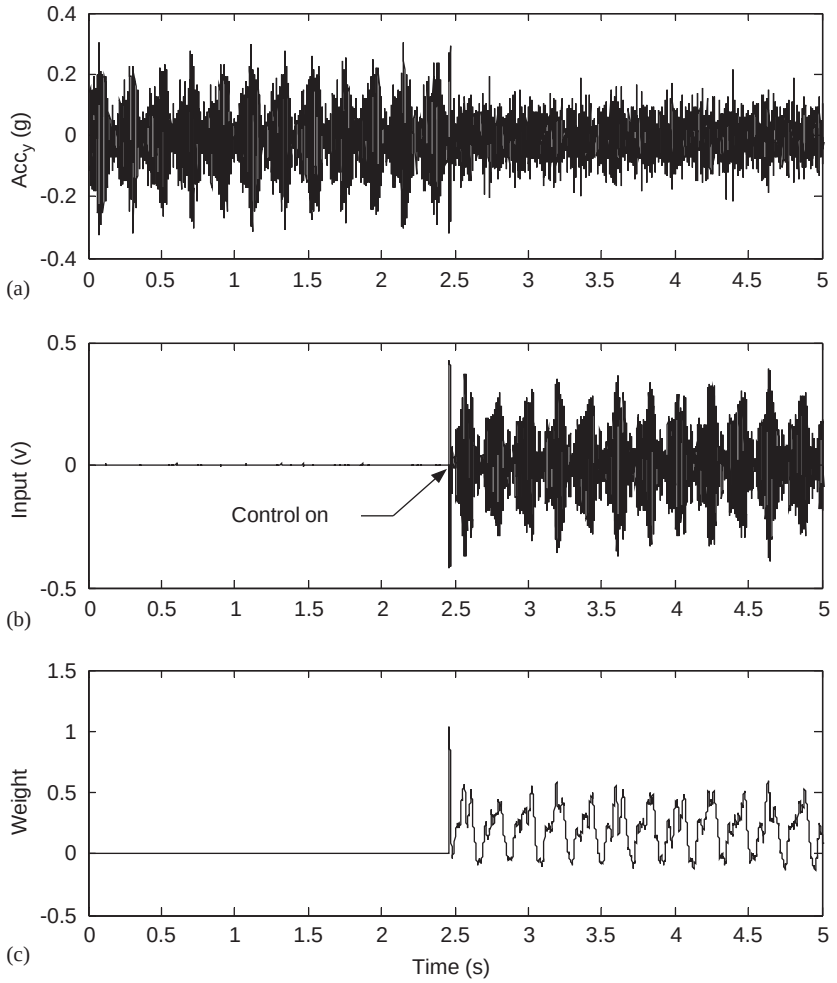

Fig. 13. The corresponding parts of time history response functions of the improved delayed-x LMS case study given in Fig. 12: (a) housing vibration in the y axis (error signal); (b) control voltage to the piezoelectric amplifier; (c) first weight of the controller.

delayed-x LMS algorithm used in Fig. 8 to that of the improved delayed-x LMS algorithm used in Fig. 14. It is clearly shown in Fig. 16 that there are several side band tones, which are due to rotation speed fluctuation. This point is consistent with the result shown in Fig. 10. Furthermore, all peaks in the frequency range between 280 and 300 Hz are reduced even though a single-speed rotation signal has been used as the reference signal. This demonstrates the ability of the LMS algorithm to track small speed fluctuation. Most importantly, the improved delayed-x LMS algorithm shows larger tonal reductions than the conventional delayed-x LMS algorithm.

To demonstrate that the active vibration control approach can be also applied to more than one harmonic, control of the housing vibrations at both the first and second operating gear mesh frequencies will now be attempted. For this case, a different rotational speed is used. Fig. 17 shows the housing vibration (Acc_y) control results for rotational speed of 220 rpm. The reference

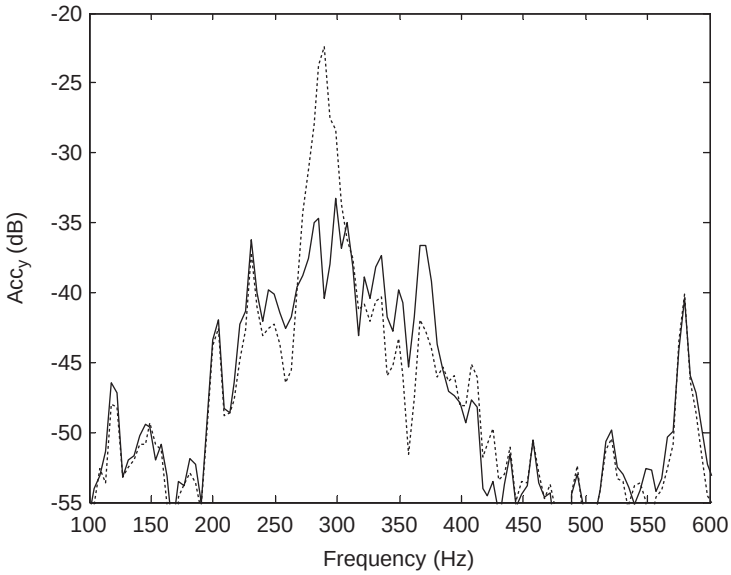

Fig. 14. Effect of the improved delayed-x LMS algorithm comprising of a 32-order FIR filter on housing vibration response spectrum along the y-axis denoted by Acc_y ($\lambda = 0.99$; dB re. 1 g; $\cdots$, control off; —, control on).

signals are chosen to be synthesized sinusoidal signals at 220 and 440 Hz. The digital multi-rate FIR filter shown in Fig. 6 is used for the error signal and the order of the controller weight for each harmonic is reduced to 16. It can be seen from Fig. 17 that the housing vibrations at both the first and second gear mesh frequencies have been successfully suppressed by about 8 dB. Even though they are not used directly as the control target, it is also interesting to examine the effect of the controller on the housing vibration perpendicular to gear line-of-action (Acc_x) and the radiated sound pressure level. These two results are shown in Fig. 18. In these plots, a 2–6 dB reduction in vibration (Acc_x) and 6–8 dB reduction in the sound pressure level at the first 2 mesh harmonics are observed. Several housing vibrations at locations other than the control position were also measured when the active control was activated. Under certain narrow rotation speeds, vibration amplifications at some of those uncontrolled locations are observed in the experiments, which might be attributed to un-modeled dynamics, such as gear housing modes, backlash and frictional forces at the mesh. Further detailed analysis of the effect of unmodeled dynamics and the secondary factors on the global vibration change will be presented in a future paper.

6. Conclusion

Based on the active shaft transverse vibration control concept formulated theoretically in a previous work, an experimental active gearbox structure applying an improved delayed-x LMS control algorithm is developed in the present study. The gearbox system is employed to evaluate the feasibility of suppressing housing vibrations at the first two gear mesh frequencies. In order to

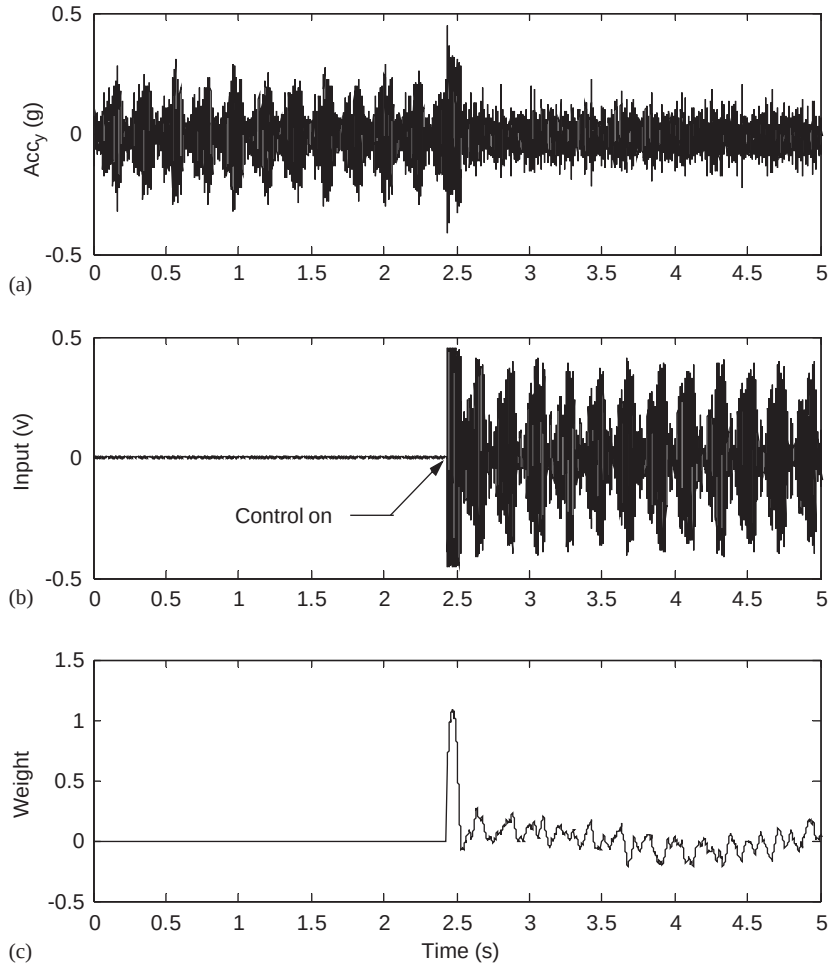

Fig. 15. The corresponding parts of time history response functions of the improved delayed-x LMS case study given in Fig. 14: (a) housing vibration in the *y*-axis (error signal); (b) control voltage to the piezoelectric amplifier; (c) first weight of the controller.

reduce the out-of-band overshoot and increase the convergence rate, two fundamental enhancements that incorporate an adaptive line enhancer and a constrained error technique are adopted. Furthermore, to avoid the use of an analog anti-aliasing filter prior to the analog-to-digital converter and to reduce the filter path delay, an over-sampling scheme and a multi-rate minimum-phase FIR filter are applied. The resultant active vibration control algorithm is successfully implemented in a PowerPC processing board and verified experimentally. The test results show up to 18 dB reduction in the housing vibration at the mesh harmonics. Additionally, the active vibration control system yields 5–8 dB in the gear whine noise at the first and second operating gear mesh frequencies. In future work, the experimental system will be applied to evaluate gear vibration and noise suppression capabilities at higher operating speeds and loads.

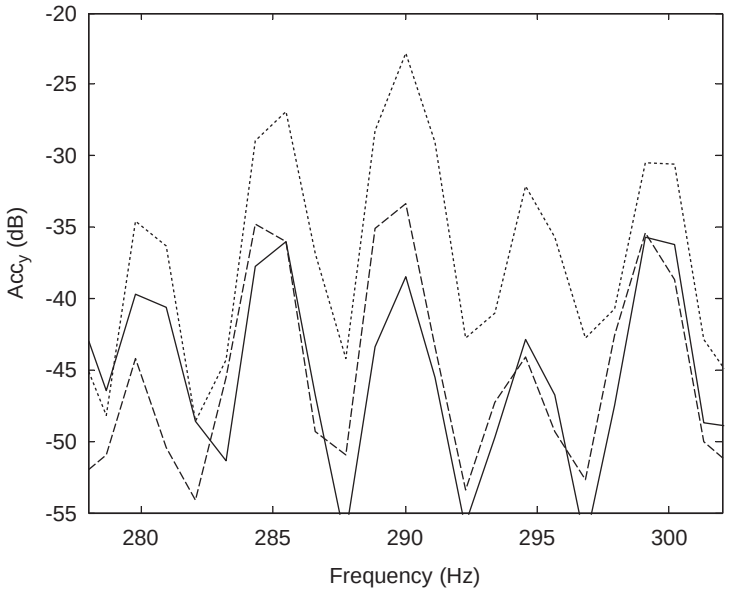

Fig. 16. Controller performance comparison of conventional and improved delayed-x LMS algorithms using FFT zoom analysis (dB re. 1 g; · · · ·, control off; - - -, control on using conventional algorithm;—, control on using improved algorithm).

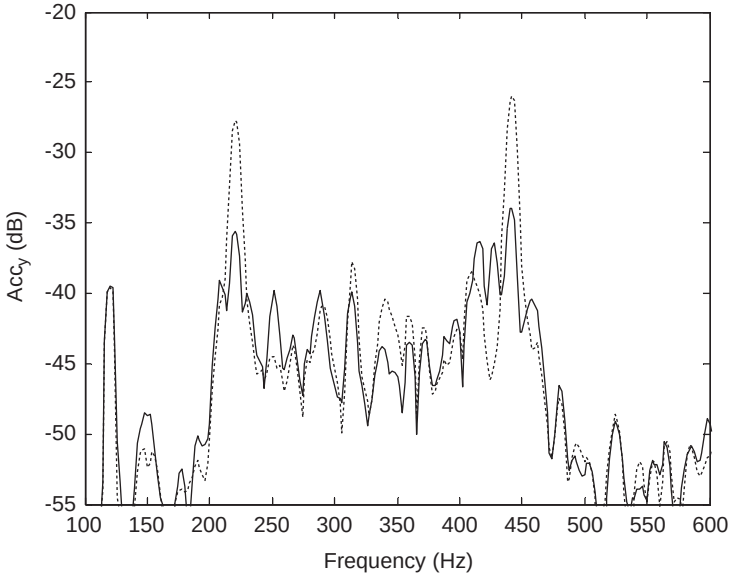

Fig. 17. Effect of the improved delayed-x LMS algorithm comprising of a 16-order FIR filter on housing vibration response spectrum along the y-axis denoted by Acc_y at 210 rpm (dB re. 1 g; · · · ·, control off; —, control on).

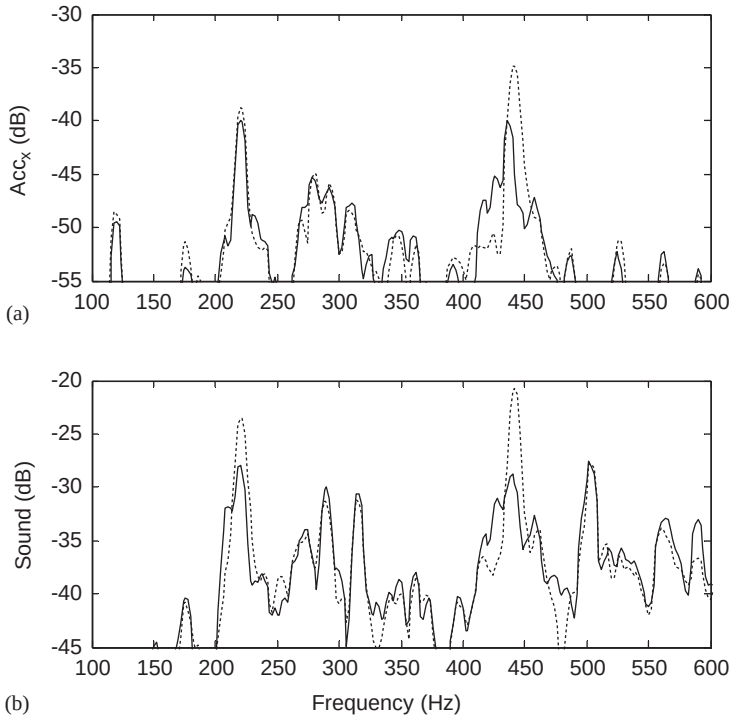

Fig. 18. The corresponding housing vibration response spectrum along x-axis denoted by Acc_x (top; dB re. 1 g) and the radiated gear whine spectrum (bottom; dB re. 1 V) at 210 rpm (· · · ·, control off; —, control on).

Acknowledgements

The material is based upon work supported by the US Army Research Office under contract/grant DAAD19-00-1-0158 (Project No. P-40942-EG-DPS). The ARO technical monitor is Dr. Gary Anderson.

References

[1] J.D. Smith, *Gear Noise and Vibration*, Marcel Dekker, New York, 1999.
[2] D.R. Houser, R. Singh, *Gear Noise Short Course Notes*, The Ohio State University, Columbus OH, 2002.
[3] G.T. Montague, A.F. Kascak, A. Palazzolo, D. Manchala, E. Thomas, Feed-forward control of gear mesh vibration using piezoelectric actuators, NASA Technique Memorandum 106366, 1994.
[4] B. Rebbechi, C. Howard, C. Hansen, Active control of gearbox vibration, *Proceedings of the Active Control of Sound and Vibration Conference*, Fort Lauderdale, 1999, pp. 295–304.
[5] M.H. Chen, M.J. Brennan, Active control of gear vibration using specially configured sensors and actuators, *Smart Materials and Structures* 9 (2000) 342–350.
[6] T.J. Sutton, S.J. Elliott, Active attenuation of periodic vibration in nonlinear systems using an adaptive harmonic controller, *Journal of Vibration and Acoustics* 117 (1995) 355–362.
[7] Y.H. Guan, W.S. Shepard Jr., T.C. Lim, Direct hybrid adaptive control of gear pair vibration, *Journal of Dynamic Systems, Measurement and Control* 125 (2003) 585–594.

[8] Y.H. Guan, M. Li, T.C. Lim, W.S. Shepard Jr., Comparative analysis of actuator concepts for active gear pair vibration control, *Journal of Sound and Vibration* 269 (2004) 273–294.
[9] T.J. Sutton, S.J. Elliott, M.J. Brennan, K.H. Heron, D.A.C. Jessop, Active isolation of multiple structural waves on a helicopter gearbox support strut, *Journal of Sound and Vibration* 205 (1997) 81–101.
[10] I. Pelinescu, B. Balachandran, Analytical study of active control of wave transmission through cylindrical struts, *Smart Materials and Structures* 10 (2001) 121–136.
[11] D.R. Mahapatra, S. Gopalakrishnan, B. Balachandran, Active feedback control of multiple waves in helicopter gearbox support struts, *Smart Materials and Structures* 10 (2001) 1046–1058.
[12] R. Maier, M. Pucher, M. Gembler, H. Schweitzer, Helicopter interior noise reduction by active vibration isolation with smart gearbox struts, *Proceedings of the Active Control of Sound and Vibration Conference*, Fort Lauderdale, FL, USA, 1999, pp. 189–198.
[13] C.C. Moon, Design and Vibro-acoustic Characterization of Gear Testing Machines for Active Vibration Control, M.Sc. Thesis, The University of Alabama, 2002.
[14] H.S. Kim, Y. Park, Delayed-X LMS algorithm: an efficient ANC algorithm utilizing robustness of cancellation path model, *Journal of Sound and Vibration* 212 (1998) 875–887.
[15] Y. Park, H. Kim, Delayed-x algorithm for a long duct system, *Proceedings of Inter-Noise 93*, 1993, pp. 767–770.
[16] S.J. Elliott, P. Darlington, Adaptive cancellation of periodic, synchronously sampled interference, *IEEE Transactions on Acoustics, Speech, and Signal Processing* ASSP-33 (1985) 715–717.
[17] S.M. Kuo, D.R. Morgan, Active noise control: a tutorial review, *Proceedings of the IEEE* 87 (1999) 943–973.
[18] C.C. Boucher, S.J. Elliott, P.A. Nelson, Effect of errors in the plant model on the performance of algorithms for adaptive feedforward control, *IEE Proceedings, Part F: Radar and Signal Processing* 138 (1991) 313–319.
[19] B. Widrow, S.D. Stearns, *Adaptive Signal Processing*, Prentice-Hall, Englewood Cliffs, NJ, 1985.
[20] S.M. Kuo, M.J. Ji, Passband disturbance reduction in periodic active noise control systems, *IEEE Transactions on Speech and Audio Processing* 4 (1996) 96–103.
[21] J. Hong, D.S. Bernstein, Bode integral constraints, *colocation, and spillover in active noise and vibration control, IEEE Transactions on Control Systems Technology* 6 (1998) 111–120.
[22] S.D. Snyder, C.H. Hansen, The influence of transducer transfer functions and acoustic time delays on the implementation of the LMS algorithm in active noise control systems, *Journal of Sound and Vibration* 141 (1990) 409–424.
[23] I.S. Kim, H.S. Na, K.J. Kim, Y.J. Park, Constraint filtered-x and filtered-u least-mean-square algorithms for the active control of noise in ducts, *Journal of the Acoustical Society of America* 95 (1994) 3379–3389.
[24] P.P. Vaidyanathan, *Multirate Systems and Filter Banks*, PTR Prentice Hall, Engelwood Cliffs, NJ, 1993.
[25] C.H. Hansen, S.D. Snyder, *Active Control of Noise and Vibration*, E.&F.N. Spon, London, 1997.